

## A meteorite crater on Earth formed on September 15, 2007: The Carancas hypervelocity impact

G. TANCREDI<sup>1\*</sup>, J. ISHITSUKA<sup>2</sup>, P. H. SCHULTZ<sup>3</sup>, R. S. HARRIS<sup>3</sup>, P. BROWN<sup>4</sup>, D. O. REVELLE<sup>5</sup>,  
K. ANTIER<sup>6</sup>, A. LE PICHON<sup>6</sup>, D. ROSALES<sup>2</sup>, E. VIDAL<sup>2</sup>, M. E. VARELA<sup>7</sup>, L. SÁNCHEZ<sup>8</sup>,  
S. BENAVENTE<sup>9</sup>, J. BOJORQUEZ<sup>10</sup>, D. CABEZAS<sup>2</sup>, and A. DALMAU<sup>2</sup>

<sup>1</sup>Dpto. Astronomía, Fac. Ciencias, Iguá 4225, 11400 Montevideo, Uruguay

<sup>2</sup>Instituto Geofísico del Perú, Lima, Perú

<sup>3</sup>Department Geological Sciences, Brown University, 324 Brook Street, Providence, Rhode Island 02912–1846, USA

<sup>4</sup>Department of Physics and Astronomy, University of Western Ontario, London, ON N6A 3K7, Canada

<sup>5</sup>EES-2, Atmospheric, Climate and Environmental Dynamics Group—Meteorological Modeling Team, Los Alamos National Laboratory,  
P.O. Box 1663, MS D401, Los Alamos, New Mexico 87545, USA

<sup>6</sup>Commissariat à l’Energie Atomique, Centre DAM—Ile de France, Département Analyse Surveillance Environnement,  
Bruyères-le-Châtel, 91297 Arpajon Cedex, France

<sup>7</sup>Complejo Astronómico El Leoncito—CASLEO, San Juan, Argentina

<sup>8</sup>Inst. Ciencias Geológicas, Fac. Ciencias, Iguá 4225, 11400 Montevideo, Uruguay

<sup>9</sup>Universidad Nacional del Altiplano, Puno, Perú

<sup>10</sup>Universidad Nacional Agraria La Molina, Lima, Perú

\*Corresponding author. E-mail: [gonzalo@fisica.edu.uy](mailto:gonzalo@fisica.edu.uy)

(Received 1 December 2008; revision accepted 12 April 2009)

---

**Abstract**—On September 15, 2007, a bright fireball was observed and a big explosion was heard by many inhabitants near the southern shore of Lake Titicaca. In the community of Carancas (Peru), a 13.5 m crater and several fragments of a stony meteorite were found close to the site of the impact. The Carancas event is the first impact crater whose formation was directly observed by several witnesses as well as the first unambiguous seismic recording of a crater-forming meteorite impact on Earth. We present several lines of evidence that suggest that the Carancas crater was a hypervelocity impact. An event like this should have not occurred according to the accepted picture of stony meteoroids ablating in the Earth’s atmosphere, therefore it challenges our present models of entry dynamics. We discuss alternatives to explain this particular event. This emphasizes the weakness in the pervasive use of “average” parameters (such as tensile strength, fragmentation behavior and ablation behavior) in current modeling efforts. This underscores the need to examine a full range of possible values for these parameters when drawing general conclusions from models about impact processes.

---

### INTRODUCTION

Extraterrestrial material (meteoroids) continually strike the upper atmosphere of the Earth at velocities over 40,000 km/h. Due to friction with the atmosphere, the smallest particles totally ablate in the upper atmosphere, leaving a luminous ionized trail. Larger particles (up to a few tons), produce bright fireballs that can be observed over extended areas and may produce sounds audible to ground-based observers. During atmospheric entry, such meteoroids largely are decelerated and usually fragment (see e.g., Ceplecha et al 1998). In some cases, a few meteorites reach the surface at very low velocities (generally close to low

terminal speed—100–300 m s<sup>-1</sup>—for multi-kilogram-ranged masses), usually producing little damage in the impacted area. Iron meteoroids with masses over a few tens of tons can reach the surface without major loss of the original mass, but weaker stony meteoroids are generally believed to need masses greater than several megatons in order to reach the surface at hypersonic velocities (Bland and Artemieva 2003). A recent crater-forming event in the Andes Altiplano of Peru, which we describe in detail, challenges this accepted “standard” picture of stony meteoroids ablating in the Earth’s atmosphere.

On September 15, 2007, about 11:45 A.M. local time (16:45 UT) (see below for a more precise estimate of the event

time), on the southern shore of Lake Titicaca close to the border between Peru and Bolivia, many inhabitants saw a bright fireball and heard explosive sounds (Fig. 1) (Macedo and Machare 2007). Ten kilometers south of Desaguadero, the villagers of the small hamlet of Carancas heard a large explosion and observed a rapidly expanding cloud of dust covering a large fraction of the sky. Some minutes later, they found a crater about 15 m in diameter at the site of the “explosion” as well as numerous blocks (with diameters less than  $\sim 1$  m) of near-surface sediments dispersed over large distances (Fig. 2). Groundwater rose to cover the crater floor within minutes with bubbles lasting several minutes after the event. Some reports mentioned that the water was boiling, but J. I. and G. T. (we will use the initials of the authors to refer to particular contribution of any of them) in one of their visits to the area interviewed the policemen that were inside the crater an hour after the impact, and they indicated that the area was not hot and it was not steaming. The water might be bubbling due to the release of gases trapped below the surface, but it was not boiling. Examination of videos of the crater made only minutes after the impact corroborate these testimonies. Some centimeter-sized pieces of material, clearly distinct from the local sediments, were found draped inside and outside the crater. Preliminary analysis of this material showed the presence of chondrules (Macedo and Machare 2007). A grey powder was widely spread on the walls of the crater. From this evidence, the event appears to represent a freshly created meteorite impact crater. Although a few craters have been formed in recent history (Table 1), the Carancas event is the first case in recorded history where the formation of the crater and the ejected material was observed directly by several witnesses.

Several aspects of this intriguing event are analyzed in the following sections: 1) the fireball and its trajectory; 2) the meteorites; 3) the crater and the ejecta; and 4) the alleged health problems that were claimed to have afflicted local residents. One of the key questions related to this event is to determine the speed of the impactor and the impact energy; in order to discuss whether this event corresponded to a hypervelocity impact or not. Here we use the terms “high velocity” or “hypervelocity impacts” to mean impacts with velocities above the sound speed in the target material, which give rise to shock waves spreading out from the impact point. This topic will be further discussed in the following sections.

### THE FIREBALL AND ITS TRAJECTORY

The intense fireball was observed in broad daylight by several witnesses in an area mostly east of the impact site (Fig. 1). Analyzing the reports, we conclude that the direction of the fireball was roughly east-west.

Unfortunately, we have very few optical records of the passage of the fireball. The only photograph, taken some minutes after the fireball proper, shows a wavy smoke trail

deformed by winds without any ground reference; it is thus unable to help in determining the path of the meteoroid. Both infrasound and seismic stations detected the shock wave accompanying the passage of the meteoroid through the atmosphere. The infrasound stations of the International Monitoring System (IMS) located in La Paz, Bolivia, (I08BO, 81 km northeast of the impact site) and in Asunción, Paraguay, (I41PY, 1620 km southeast of the crater) recorded airwaves associated with the fireball. Five regional seismic stations located close to La Paz (operated by the Observatorio San Calixto, see Minaya et al. (2007) for a description of the network) and one in Peru (operated by Instituto Geofísico del Perú) detected ground-air coupled arrivals from the atmospheric flight and, in a few recordings, the body and surface waves generated by the impact on the ground (Fig. 3). Figure 3B is the first unambiguous seismic recording of a meteorite impact on Earth. Brown et al. (2008) and Le Pichon et al. (2008) independently obtained trajectory solutions using the infrasound and seismic data; the first team locates the fireball radiant at an azimuth of  $82^\circ$  (clockwise from the north and relative to the crater position) with a  $63^\circ$  entry angle with the horizontal; the second group found a solution with a  $110^\circ$  azimuth and a  $50^\circ$  elevation. They both estimated the impact time as being close to 16h40m17s UT (see a revision of the impact time below). Both estimates have wide error margins, generally encompassing the best fit estimate from the other work. The energy of the blast close to or at the surface, based on airwave measurements, was estimated by the previous authors as  $\sim 1\text{--}3$  tons TNT. Independent of these blast yield estimates from far-field acoustic wave measurements, in the section The Size, Mass, and Impact Energy of the Projectile we will use blast effects proximal to the crater as another gauge of the source energy.

Another data set that could be useful for the analysis of the fireball trajectory is the information provided by the witnesses. A few testimonies of witnesses in an area covering several tens of km from the impact site were collected in the days after the impact (Gonzalo Pereira, personal communication). These testimonials include (see map in Fig. 1):

1. The witnesses located between Desaguadero and Azafranal, facing south, observed the bolide heading from left to right. A detailed description of the trajectory was provided by Mr. R. Carbajal. He observed the fireball trajectory from NE to SW.
2. There are two sets of reports from the people in Guaqui: ones saw the bolide descending directly overhead and then, facing south, the fireball moves to the right. The others (closer to the Lake Titicaca) saw the bolide over the hills that are in the southern direction and going from left to right.
3. In the Communities of Corpa and Yahuri Khorawa (10 km north of Santiago de Machaca), facing north, they saw the bolide moving from right to left.

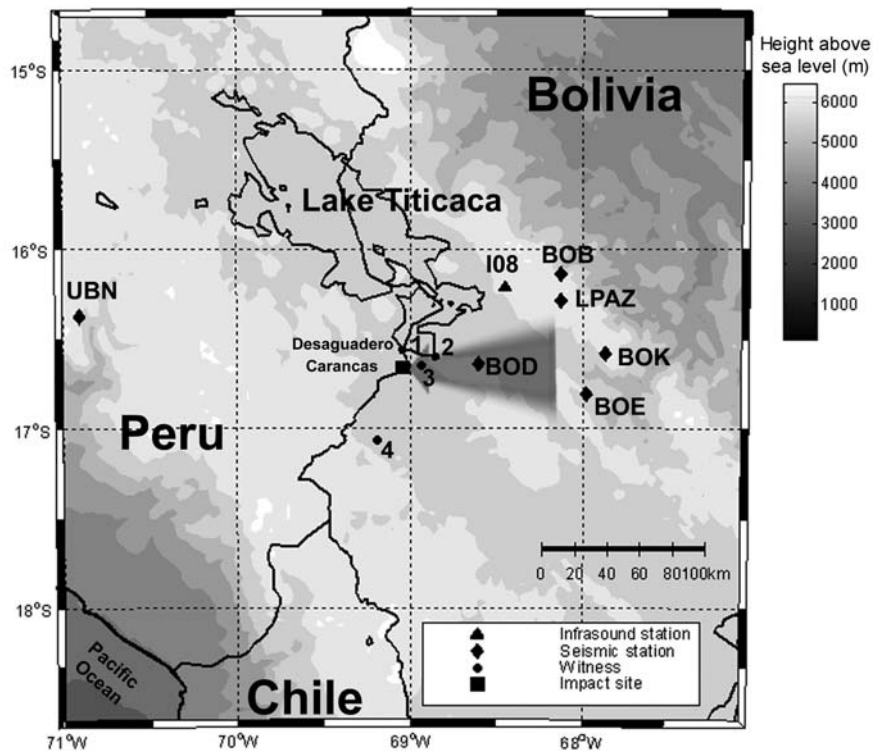


Fig. 1. Map of the region. The locations of several stations that recorded the event are shown in the map: the infrasound station of the International Monitoring System (IMS) located in La Paz, Bolivia (I08BO); five regional seismic stations located close to La Paz (BOB, BOD, BOE, BOK, and LPAZ) and one in Peru (UBN). The light-gray arrow corresponds to the probable direction of the fireball. The location of the crater was Lat: 16°39'52''S, Long: 69°02'38''W, Elev: 3 824 m a.s.l. The numbers corresponds to the following towns: (1) Desaguadero, (2) Guaqui, (3) Azafranal, (4) Santiago de Machaca.

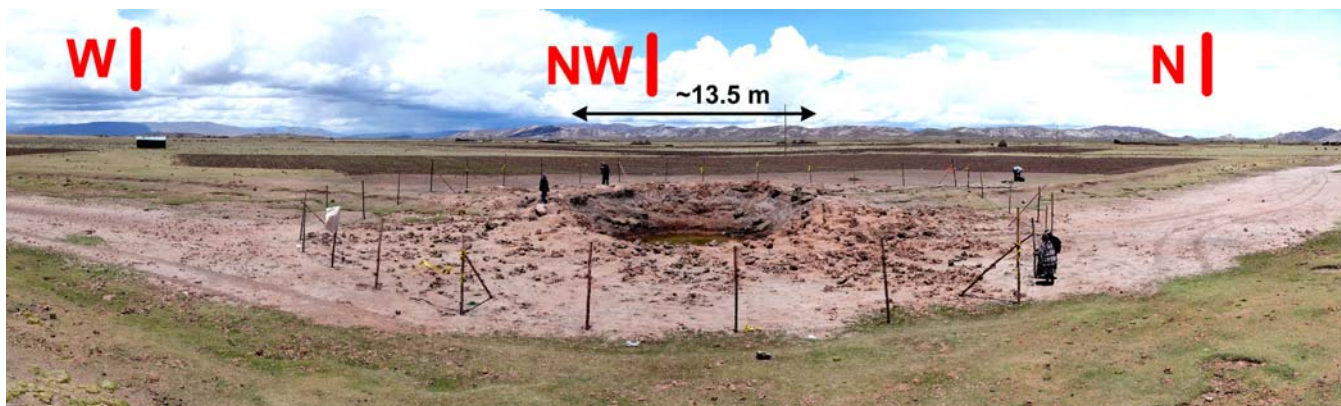


Fig. 2. Wide-field photo of the crater.

Table 1. Data taken from the articles listed in References as well as from the Meteoritical Bulletin Database (<http://tin.er.usgs.gov/meteor/>)

Year	Location of the crater	Diameter of largest crater	Number of craters or pits	Total mass of found meteorites	Meteorite type	Ref.
1998	Kunya-Urgench, Turkmenistan	6 m	Single	1.1 tons	Chondrite H5	1
1990	Sterlitamak, Russia	10 m	Single	0.3 tons	Iron IIIAB	2
1976	Jilin, China	4 m	Multiple	4 tons	Chondrite H5	3
1947	Sikhote-Alin, Russia	26.5 m	Multiple	23 tons	Iron IIAB	4

1–Mukhamednazarov (1999); 2–Petaev (1992); 3–Academia Sinica (1977); 4–Krinov (1971).

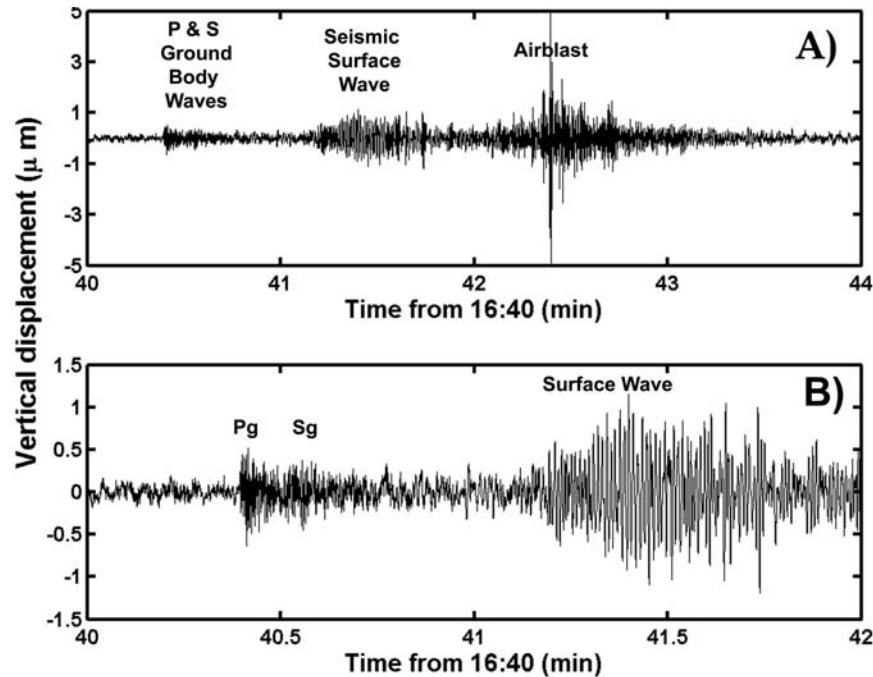


Fig. 3. Seismic signal at station BBOD of the Bolivian regional seismic network. At a distance of 47 km, BBOD location was the closest station to the impact site. The data shown is the unfiltered vertical component displacement of the short-period seismometer. The other recordings can be found in Brown et al. (2008) and Le Pichon et al. (2008). a) The recording starts at 16:40 UT and lasts 4 minutes, with vertical amplitude that almost cover the total displacement. The maximum peak-to-peak displacement is 8.6  $\mu\text{m}$ . b) A zoom of the first two minutes of the previous. We notice the P and S crustal seismic waves arrival; then, the surface waves arrival and eventually the signal of the ground-air coupled airwave arrivals. The latest low-frequency surface wave train is typical of shallow seismic events propagating in water-saturated soils. This arrival is likely related to the impact. However, its unexpected long duration ( $\sim 1$  minute) may also be explained by the acoustic-to-seismic coupling of the shock waves induced by the hypersonic shock of the meteoroid passage through the atmosphere (Kanamori et al. 1991; Hedlin et al. 2008).

These witnesses reports are in broad agreement with the trajectories mentioned above.

In order to discuss the plausibility of the different solutions, we computed a set of geocentric radiants centered on the apparent radiant position ( $Az = 80^\circ \pm 30^\circ$ ,  $Alt = 60^\circ \pm 30^\circ$ ) and pre-atmospheric velocities ranging from 12 to 18  $\text{km s}^{-1}$ , typical of NEAs approaching the Earth. In Fig. 4, we plot the set of possible geocentric radiants in an equatorial frame for the impact time, with a central meridian passing through the Sun (Tancredi et al. 2008). The different sets of solutions are marked with different symbols (see caption). The big dot corresponds to the location of the Sun and the anti-Sun in this geocentric frame. We compare the location of these solutions with the expected locations of radiants for Earth-crossing asteroids. The expected location of the radiants of NEAs are computed from the orbital elements of the known objects, according to the method presented by Tancredi (2006) (the list of NEAs is taken from the list provided by Minor Planet Center as of November 14, 2008). In Fig. 4, we also plot these possible radiants with small black dots. The distribution of NEA's theoretical radiants is clearly not isotropic; it presents a concentration toward the direction of the Sun and the anti-Sun. This characteristic has already been observed for the sky-plane distribution of Earth-crossing

asteroids (Bowell and Muinonen 1994) and it is the reason why the NEA's sky surveys generally favor the opposition direction for their search. By comparing our set of solutions (large symbols) with the radiants of known NEAs, we conclude that only the solutions of high altitude (i.e.,  $Alt > 45^\circ$ ) are compatible with NEAs' orbits.

All solutions have low orbital inclinations ( $i \leq 5^\circ$ ), and the low-velocity ones have aphelia inside Jupiter's orbit, a condition generally associated with meteorite-producing fireballs (e.g., Wetherill and ReVelle 1981). Therefore, we favor the solutions with pre-atmospheric velocities  $v \leq 16 \text{ km s}^{-1}$ , apparent radiant  $Az \sim 80\text{--}110^\circ$  and  $Alt \geq 45^\circ$ .

### Reanalysis of the Seismic Data

We have fused all the data recorded by the infrasound and seismic stations that was initially independently studied by Brown et al. (2008) and Le Pichon et al. (2008). Table 2 presents the list of the stations that recorded at least one signal from the Carancas event. We perform a new analysis of the data in order to have a more precise estimate of the impact time.

The impact of the meteorite on the ground was detected via body waves at the five closest seismic stations with

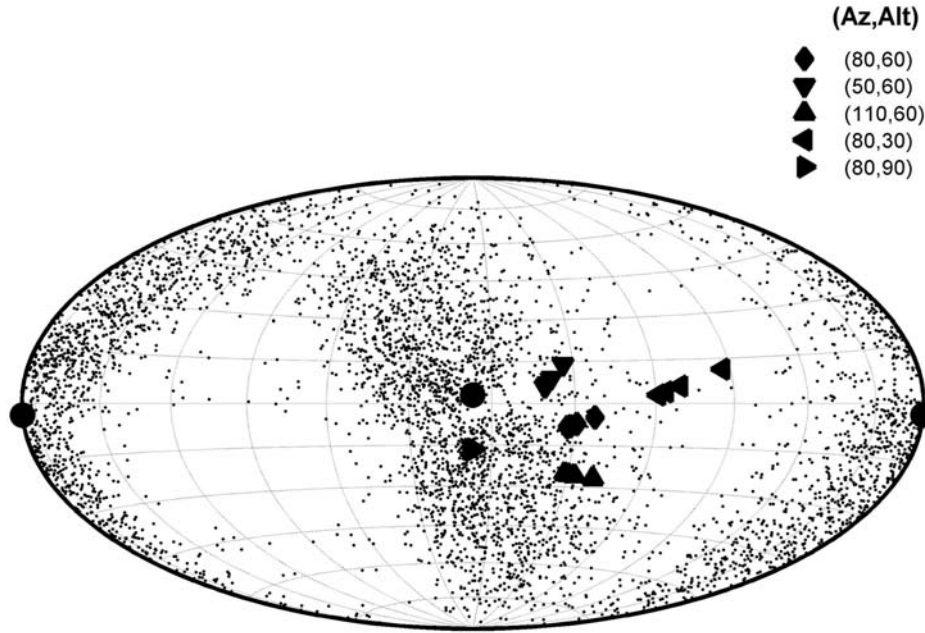


Fig. 4. Radiants in equatorial coordinates of a set of possible solutions and NEAs. The + signs correspond to the nominal solution ( $Az = 80^\circ$ ,  $Alt = 60^\circ$ ), and the different oriented triangles correspond to alternative solutions (the values of the azimuth and altitude are listed in the upper right of the figure). Among the same symbols, the different points correspond to different geocentric velocities. The points from right to left correspond to velocities of 12, 14, 16, and 18  $\text{km s}^{-1}$ , respectively. The big black circle close to the center corresponds to the position of the Sun at the moment of impact and the two black circles  $180^\circ$  apart is the position of the anti-Sun. The small black dots are the locations of the NEAs' radiants.

Table 2. Name, coordinates, and distances from the crater of the studied short-period vertical seismic sensors (LPAZ, BBOB, BBOD, BBOE, BBOK, UBINS) and the two IMS infrasound arrays (I08BO-Bolivia and I41PY-Paraguay). They are listed in order of distance to the crater.

Station	Longitude ( $^\circ\text{W}$ )	Latitude ( $^\circ\text{S}$ )	Elevation (m a.s.l.)	Distance from crater (km)
BBOD	68.6	16.64	4235	47
I08BO	68.45	16.21	4131	80
LPAZ	68.13	16.29	4095	105
BBOB	68.13	16.14	3911	112
BBOE	67.98	16.81	4325	114
BBOK	67.87	16.58	4638	125
UBINS	70.90	16.37	5670	232
I41PY	57.31	26.34	164	1617

Table 3. Observed arrival times (UT) of the Pg-waves at five different stations among the listed in Table 2.

Station	Arrival time Pg (UT)
BBOD	16:40:23.5
LPAZ	16:40:35.4
BBOB	16:40:35.8
BBOE	16:40:36.3
BBOK	16:40:39.2

distances ranging from 47 up to 125 km from the impact site. A seismogram (recorded by the closest station, BBOD) is presented in Fig. 3.

At short range from the impact site, two kinds of arrivals can reach the stations: at very close distance, the crustal P-wave arrival that transmits through the crust is the first phase

to reach the station (Pg); after a critical distance, the P-wave refracted at the Mohorovicic discontinuity (Pn) can be the first phase reaching the station. This critical distance is given by:  $r_{crit} = 2h \sqrt{[(v_2 + v_1) / (v_2 - v_1)]}$  (Lillie1999); where  $h$  is the depth of the Moho,  $v_1$  and  $v_2$  are the P-wave velocities in the crust and in the Moho, respectively. Typical values of  $v_1$  are between 5–6  $\text{km s}^{-1}$  and for  $v_2$  are 8  $\text{km s}^{-1}$ . Since the Moho is very deep below the Altiplano ( $h \sim 70$  km; Yuan et al. 2002), the critical distance is over 200 km in this area. Therefore, we expect all stations to have detected the Pg-body wave first.

Table 3 lists the observed arrival times of the body waves for the 5 different stations.

Assuming a rectilinear path in the crust, the arrival times ( $t_i$ ) for each station is related with the distance to the

epicenter ( $d_i$ ), the velocity ( $v$ ) and the impact time ( $t_0$ ), through the following equation (one equation per station):

$$t_o + d_i/v = t_i. \quad (1)$$

Since we know the exact location of the epicenter, i.e., the impact site, we then have an over determined system of linear equations with two unknowns: the inverse of velocity ( $1/v$ ) and the impact time ( $t_0$ ). The system of equations is solved with the *lsqlin* method in Matlab, which solves linear least-squares problems. For the arrival times of the Pg-wave listed in Table 3, we obtain a new estimate of the impact time of 16:40:14.1 UT and a velocity for the Pg-wave of  $5.1 \text{ km s}^{-1}$ . This impact time is slightly different from the estimates made by Brown et al. (2008) and Le Pichon et al. (2008). The value obtained by (Brown et al. 2008) is computed from the arrivals of the airblast; the uncertainties for this type of estimation are generally large. Le Pichon et al. (2008) assumed a two-layer regional velocity model, and they solved simultaneously for the location of the impact and the time; they obtained a location of the impact source 8 km from the crater. Instead, we have assumed a known impact location and solved for the impact time.

This new precise impact time could be useful to put constraints in the impact speed, if one is able to get an estimate of the fireball time. This might be possible from a reanalysis of the infrasound data or from a detection of the fireball by satellite systems.

### THE METEORITE

Several samples of the grayish material found close to the crater were collected a few minutes after its formation. Petrographic and electron microprobe analysis were performed on two thin sections of small meteorite fragments. The samples were investigated with an optical microscope and analytical scanning electron microscope JEOL 6400. Major element composition was determined with an ARL-SEM-Q electron microscope (Naturhistorisches Museum, Vienna, Austria) operated at 15 kV accelerating voltage and 15 nA sample current. The on-line ZAF program was used for corrections. Figure 5 presents some microphotographs of the Carancas meteorite. The several well defined chondrules (round objects observed in the lower right corner, central upper part and left side of Fig. 5A) are mainly composed of pyroxenes. Two radiating pyroxene chondrules are also observed (white arrows) as well as several euhedral olivines (e.g., clear crystal below the chondrule in the central upper part of the image). All black irregular grains in all images correspond to metal and sulfides. Their chondrule texture, minor amount of clinopyroxene as well as their relatively uniform composition of olivine and pyroxene grains (ferrosilite in orthopyroxene: mol% 16.7; fayalite in olivine: mol% 18) classify the Carancas meteorite as an H4–5 ordinary chondrite, in concordance with Connolly (2007).

We compute the bulk density of the meteorite by measuring its mass and estimating its volume with a variant of the Archimedean method (we half fill a recipient with water, the volume of the meteorite is the mass of the recipient with and without the meteorite inside, divided by the density of the water, i.e.,  $1 \text{ g/cm}^3$ ). For the measurements we use a meteorite sample of 4 g. collected by J. I. outside the crater, in the first days after the impact. An analytical scale with a precision of 0.001 gr. was used. Measurements of the bulk density of a meteorite sample gave a value of  $3.50 \times 10^3 \pm 0.01 \times 10^3 \text{ kg/m}^3$ . This value is within the range of bulk densities of several H chondrites measured by Britt and Consolmagno (2003).

A large number of small meteoritic pieces were also collected the days following the impact, mainly by local residents. Most fragments were within tens of meters of the southwest rim of the crater. Although the total amount of collected material is unknown, we estimate that less than a few kilograms of meteoritic material in total were removed, based on videos and interviews of residents and local authorities.

Rosales et al. (2008) conducted a magnetometer survey to identify large fragments of the original main meteorite impactor potentially remaining beneath the crater. They found small geomagnetic anomalies that could be associated with fragments of the original impacting meteorite. The peak values where  $T_{\min} = -11 \text{ nTesla}$  and  $T_{\max} = +17 \text{ nTesla}$ . On a meteorite sample of 28 g, they also measured the remnant magnetization per unit volume:  $I_r = 0.21 \text{ gauss}$ . In case a meteorite fragment of diameter ( $D$ ) was present below the surface at a depth ( $r$ ), the amplitude of the magnetic measured on the surface should be given by the following equation (Breiner 1999):

$$T_r = \frac{T_{\max} - T_{\min}}{2} = \frac{2M_r}{r^3} = \frac{\pi I_r D^3}{3r^3}. \quad (2)$$

Inputting the values presented above in the previous equation, we estimate that a single fragment of meteoritic material larger than half a meter in diameter is unlikely to be below the crater at depth above  $\sim 5 \text{ m}$ .

We believed that most of the original  $\sim 1 \text{ ton}$  projectile (see below for this mass estimate) was heavily fragmented and dispersed at impact. We recall the observation, in the first days after impact, of a grey powder spread on the walls of the crater that represents the bulk of the original mass of the original meteorite. As of late 2008, no excavation or deep trenching of the remains of the crater has been performed.

### THE CRATER

The impact occurred in a dry stream (arroyo), but the crater excavation also included its adjacent stream bank (Fig. 2). At the time of impact, the arroyo was dry, but sands were water-saturated  $\sim 1.5 \text{ m}$  below the surface. Grassy topsoil extended irregularly over the stream bed from the stream bank. The stream embankment has approximately  $1 \text{ m}$

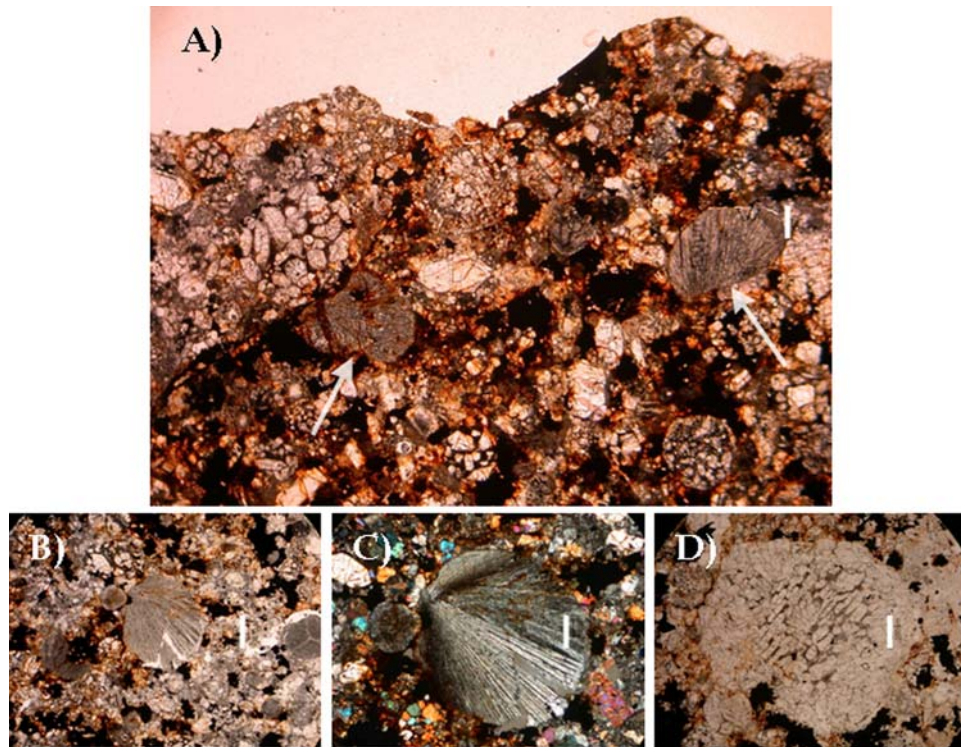


Fig. 5. A) Transmitted light optical image showing the texture of the Carancas H4–5 ordinary chondrite. Scale (longitudinal white bar): 400  $\mu\text{m}$ . B) In the center is a radiating pyroxene chondrule in plane-polarized light. Scale: 400  $\mu\text{m}$ . C) Detail of the radiating pyroxene chondrule in cross-polarized light. Scale: 200  $\mu\text{m}$ . D) Olivine rich object characterized by having a barred olivine texture in the center (olivine: light grey and recrystallized mesostasis: medium grey) and a thick olivine rim (light grey). Image in plane-polarized light. Scale: 200  $\mu\text{m}$ .

elevated topography with a fully developed soil sequence: tightly matted grassy surface on top of an organic clay layer, which is over another layer containing calcium carbonate. The western crater rim is significantly higher than the eastern rim due to this local, pre-impact topography. A sketch of the crater showing the topography and the relevant dimensions of the structure can be found in Tancredi et al. (2008) and Le Pichon et al. (2008). The crater had a mean diameter of 13.5 m and a very small ellipticity. The depth of the modified (water and sediment-filled) crater measured from the lowest rim was 2.4 m, with a depth-to-diameter ratio of 0.18. Soon after the impact (based on the videos), several large ~1–2 meter-sized spall blocks slid down from the over-steepened western rim of the crater. On this rim, a few large flaps (>20 cm in size) remained hinged, either flipped over or steeply dipping. A grey powder coated the western wall and rim. By contrast, the eastern wall which had initially low elevation was covered by smaller (<20 cm in size) blocks (Fig. 2). Additionally, a wedge-shaped gap (~30°) in blocky ejecta extended from the eastern rim, which is believed to be the up range direction relative to the fireball trajectory.

At issue, however, is whether this crater was produced by a low speed penetration funnel or by a high speed shock (explosive energy transfer).

On the flanks of the WNW to NW rim (approximately downrange) the largest meter-size ejecta blocks are

overturned and resting in a blanket of fine (Fig. 6), powdery material 30 to 50 cm thick. Overturned ejecta blocks are riddled with embedded fragments of the impactor (Figs. 7A and 7B). Fragments are exposed along weathered upper surfaces but also occur several centimeters below the surface. Some cm-size fragments of similar caliche-rich target material ejected farther from the crater also contain small, embedded meteoritic fragments (Fig. 8). Because they are magnetic, some of this material probably has been mistakenly attributed to weathered meteorite fragments. Close inspection, however, reveals that such pieces contain significant terrestrial target material, i.e., are actually small impact breccias (Harris et al. 2008a). Tiny (1 mm) mixed breccias, some coated with minor amounts of melt, also were collected between 10 and 50 m from the crater (Harris et al. 2008b). Figures 8A–D shows examples of small impact breccias collected up to 50 m outside the crater. They are mixtures of meteoritic fragments and terrestrial material. Note in Fig. 8B that the meteoritic core of the particle in Fig. 8A has partially melted along the edges and wrapped around quartz and carbonate grains from the target sediments. In Fig. 8D we show that the particle of Fig. 8C is breccia composed of shattered H chondritic material mixed with terrestrial target material, including organic clasts. The implantation or injection of impactor fragments into strata derived from beneath the pre-impact surface is in agreement

with the hypothesis that the bolide was largely intact (or tightly packed) when it struck. It is also consistent with the absence of any observed accompanying shower of debris. The fragmented and pulverized impactor mass likely lined the crater wall during excavation, some of which were injected below the surface spalls.

During first contact and penetration, at least a small envelope of target material would have experienced shock pressures sufficiently high to cause mineral deformation. The most highly shocked materials should have been ejected far beyond the crater rim or directly beneath the path of the meteorite (inside the crater). The former are likely dispersed too widely to be recovered. Shocked materials on the crater floor would have been buried by, diluted by, or mixed with slumped wall rocks and washed in debris, which experienced very low to no shock conditions. Moderately shocked materials, however, would have been entrained in the ejecta cloud advancing across the surface.

Epoxy grain mounts and oil immersion slides were prepared from representative powdery proximal ejecta and consolidated ejecta blocks. For comparison, a ~2 m deep section of arroyo strata was sampled far from the crater. In the majority of the latter samples, less than 1 in 100 quartz grains exhibit any type of lamellar deformation microfabrics. Those that are observed are most similar to tectonic deformation lamellae and {10–11} growth twins. Samples taken from the downrange ejecta blanket (about 4 meters from the rim) are the notable exception (Figs. 7A and 7B). The top layer (10 cm) of ejecta shows no remarkable characteristics. Material from the next 10 cm (10–20 cm below the surface), however, exhibits occasional evidence of mineral deformation, comparable to that seen in other parts of the ejecta field and in the background sediments. Small (<0.5 mm) fragments of the meteorite also occur in this section. Farther down in the final 10 cm section (20–30 cm below the surface), about 1 in 20 (or better) quartz grains have evidence of deformation.

The styles of deformation range from single and multiple sets of wavy, continuous, and discontinuous lamellae deformation to one to three sets of significantly more planar features (Figs. 7C and 7D). The most common planar features are parallel to (0001) and are similar to basal microstructures produced at relatively low shock pressures (~5 GPa) during experimental hypervelocity impacts into loosely consolidated sedimentary targets (Stöffler et al. 1975). The experimental conditions required to produce those features ( $v = 3$  to  $5 \text{ km s}^{-1}$ ) are comparable to speeds derived for the Carancas impact ( $2\text{--}4 \text{ km s}^{-1}$ ) consistent with eyewitness accounts, as well as seismic and infrasound data and modeling (Brown et al. 2008; Le Pichon et al. 2008). Some grains contain multiple sets of planar microstructures generally parallel to (0001) and {10–13} or {10–11}. Although a few (e.g., Fig. 7D) optically resemble planar deformation features (PDFs) indicative of shock pressures exceeding ~10 GPa (Stöffler and

Langenhorst 1994), many may represent basal and rhombohedral twins developed at lower pressures, i.e., ~3 to 7 GPa (Harris et al. 2008b). These may be precursors to full PDF formation. It is important to emphasize that the concentration of grains exhibiting Böhm lamellae, {10–11} Brazil twins, and mosaicism are significantly higher in this section than other samples. This observation indicates that even lower level deformation (~1–3 GPa) associated with the impact event occur in the ejecta, rather than prior endogenic processes.

Consequently, we can confirm that Carancas represents a hypervelocity ( $3\text{--}5 \text{ km s}^{-1}$ ) impact (rather than low-speed compression), as previously suggested (Brown et al. 2008; Le Pichon et al. 2008; Harris et al., 2008a, 2008b; Schultz et al. 2008). In this work we have presented the following lines of evidence to support this conclusion: 1) the distribution of materials within the sediments; 2) intimate mixing of target and meteoritic materials in even small ejected impact breccias; 3) consistency with the inferred level of shock deformation in minerals at certain levels within the ejecta deposits; 4) the geophysical measurements of the seismic source energy (equivalent of a 1–3 tons TNT explosive event) (Brown et al. 2008; Le Pichon et al. 2008), as well as similar energy values derived from proximal blast measurements (see later); and 5) eyewitness accounts which state that the impactor continued to be luminous to ground level, a condition generally accepted to require velocities in excess of  $3\text{--}4 \text{ km s}^{-1}$  (Ceplecha et al. 1998).

Although the meteorite was strongly decelerated during atmospheric entry, the impact velocity exceeded  $3 \text{ km s}^{-1}$  and generated peak pressures in the sediments up to a few GPa. The meteoritic mass penetrated deeply at a high speed while coupling its energy to the subsurface. The energy deposited produce effects like: surface spalls, inverted rim ejecta, injection of meteoritic debris between contrasting soil horizons, long crater rays (>20 crater diameters), and excavation of horizons not exposed on the surface. The extended meteoritic debris downrange to the west is consistent with a reflected shock back into the projectile while retaining part of its initial momentum (Schultz et al. 2008).

In regard of the data presented in this section, we conclude that the Carancas event was not an atmospheric percussion crater. It also cannot be considered as an impact pit or penetration hole. The Carancas crater was a hypervelocity impact.

### The Size, Mass, and Impact Energy of the Projectile

Some estimates of the impact energy come from the analysis of the size of the crater and the use of previously published crater energy relations that determine its size as a function of the properties of the projectile and the target, i.e., crater scaling laws (Holsapple and Housen 2007). The



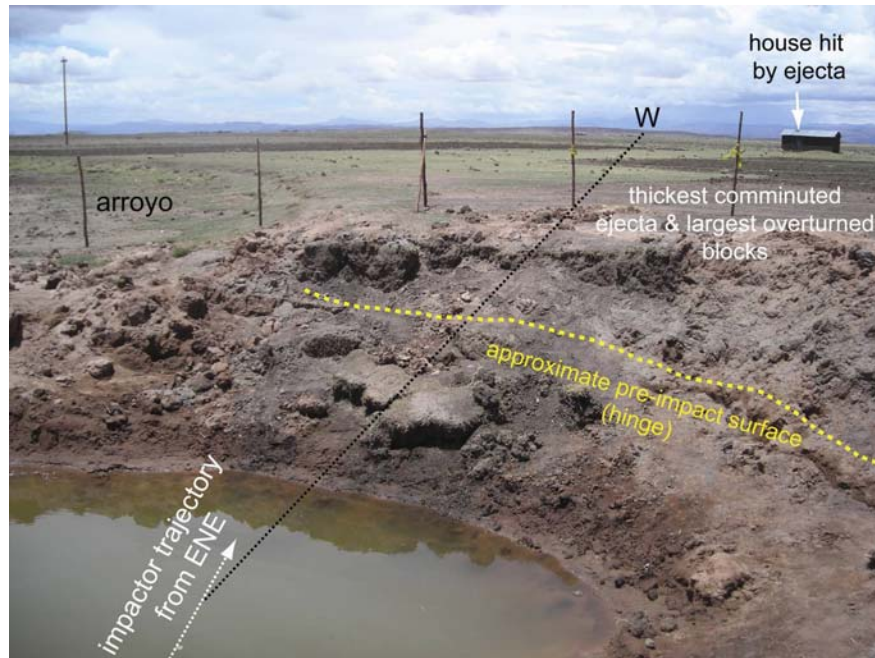


Fig. 6. Photograph of the Carancas crater centered on the western wall. E-W line (black) is shown for reference. The largest spallation blocks and thickest accumulations of finely comminuted ejecta (approximately 50 cm thick) are located behind the WNW to NW rim.

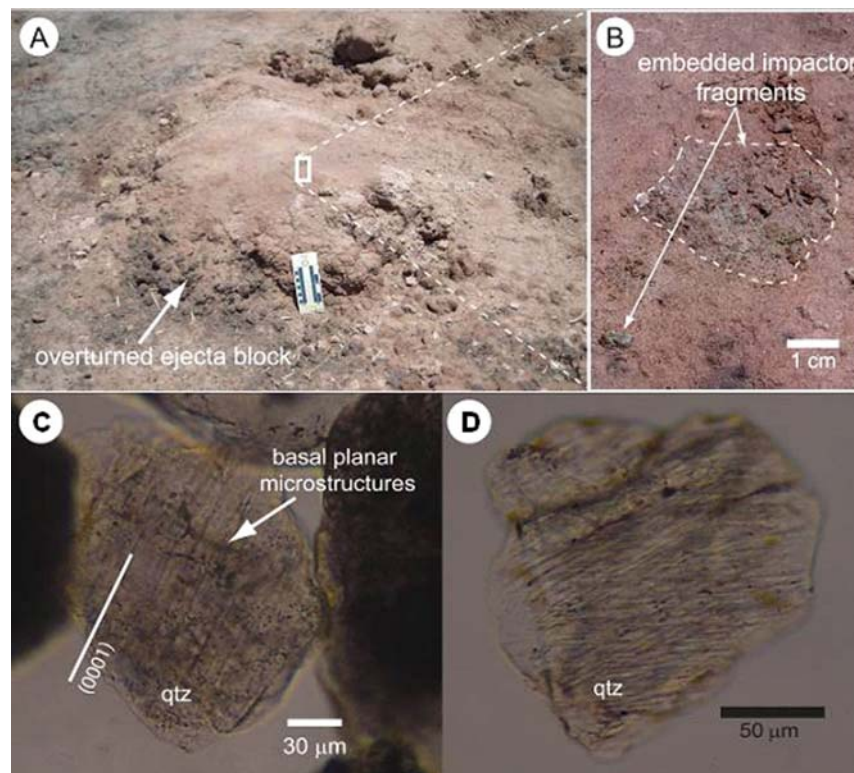


Fig. 7. A) Photograph of a large overturned ejecta block ~3 meters outside the NW rim of the Carancas crater. The dark, organic-rich A soil horizon is crushed beneath the B horizon, composed of caliche and carbonate-cemented silty sediments. The block is riddled with meteorite fragments ranging from millimeters to several centimeters wide. B) Close-up photograph of the outlined section of the ejecta block showing two of the embedded meteorite fragments. C) Plane-polarized light photomicrograph (PPL) of a quartz grain containing basal (0001) planar microstructures similar to those formed by relatively low shock pressures in experimental (e.g., Stöffler et al. 1975) and natural (e.g., Stöffler and Langenhorst 1994) hypervelocity impacts. D) Photomicrograph (PPL) of a quartz grain exhibiting at least two sets of planar microstructures.

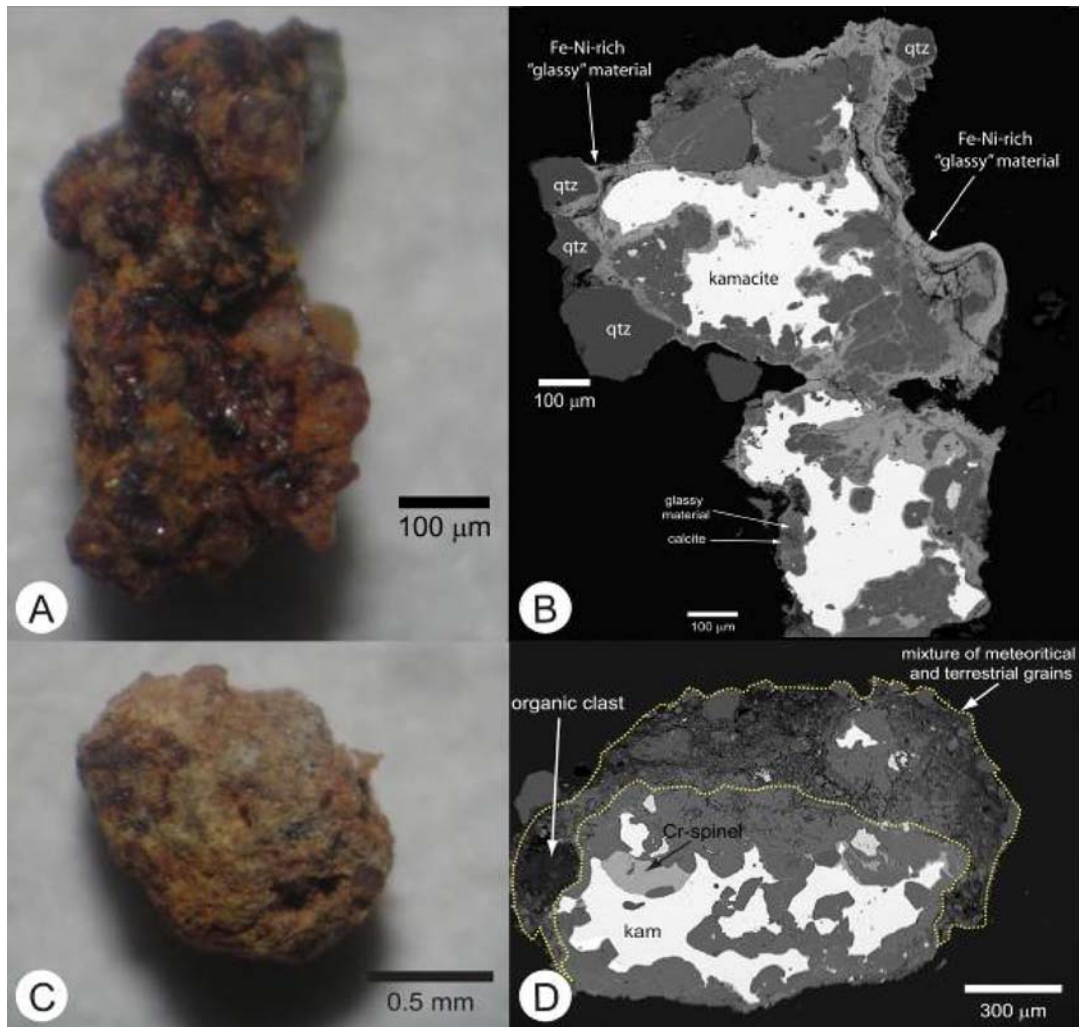


Fig. 8. Miniature impact breccias. A) Photograph of glassy ejecta found ~10 m from the Carancas crater. B) Backscattered electron (BSE) micrograph of a polished section of the ejecta particle. C) Photograph of a round lapillus-like ejecta particle collected ~50 m from the crater. D) BSE image of the previous particle.

general equation for the final crater radius ( $R$ ) divided by impactor radius ( $a$ ) for an impact into different type of targets is (Holsapple and Housen 2007):

$$\frac{R}{a} = K_1 \left[ \frac{ga \left(\frac{\rho}{\delta}\right)^{\frac{2\nu}{\mu}}}{U^2} + \left(\frac{Y}{\rho U^2}\right)^{\frac{2+\mu}{2}} \left(\frac{\rho}{\delta}\right)^{\frac{\nu(2+\mu)}{2}} \right]^{\frac{\mu}{2+\nu}}. \quad (3)$$

The equation depends on material properties like the projectile density ( $\delta$ ), the target density ( $\rho$ ), and the strength of the target material ( $Y$ ).  $g$  is the acceleration of gravity on the surface and  $U$  the normal impact speed.  $K_1$ ,  $\mu$  and  $\nu$  come from experiments (see the database in Holsapple 2003). The normal impact speed is computed with the impact angle ( $\theta$ ) as  $U = U_0 \sin \theta$ ; where  $U_0$  is the impact speed. The crater radius given in Equation 2 is the transient radius; the rim-to-rim diameter ( $D_f$ ) of the final crater is  $D_f = 2 * 1.3 * R$ .

Since the upper 1 m of the target material was a

consolidated dry soil, but water-saturated sands occur about ~1.5 m below the surface, we consider values of the strength corresponding to dry and wet soils (Holsapple and Housen 2007). An impact angle of  $60^\circ$  is assumed according to the computed trajectory (Brown et al. 2008).

The values of the parameters involved in Equation 3 that we use in our calculations are presented in Table 4.

In Fig. 9A we present a plot of the crater diameter as a function of the impactor diameter for different values of the impact speed (for 1, 3, and 6 km  $s^{-1}$ ) and the two types of soils (full line for dry soils, dashed line for wet soils). A horizontal dash-dotted line for a crater diameter of 13.5 m, corresponding to the Carancas case, is also shown. By reading back in the  $x$ -axis, we then obtain the values of the impactor diameter that would create a 13.5 m crater. The impact event is close to the limit between strength and gravity-dominated impact regime; hence, the cratering laws have some degree of uncertainty. For the velocity range between 3 and 6 km  $s^{-1}$ ,

Table 4.

Parameter values used in the cratering laws	
Impactor properties	
density (kg m <sup>-3</sup> )	3500
Target properties	
Dry soil (1)	
density (kg m <sup>-3</sup> )	1700
K <sub>1</sub>	1.03
μ	0.41
n	0.4
Y (Pa)	2e5
Wet soil (1)	
density (kg m <sup>-3</sup> )	2100
K <sub>1</sub>	0.93
μ	0.55
v	0.4
Y (Pa)	5e5
Impact angle	60

(1) Values taken from Holsapple and Housen (2007) and Holsapple (2003) and used in Equation 3. See text for the symbols.

the projectile (at impact) should have a diameter between 0.5–1.1 m, and a mass of  $\sim 0.2\text{--}3 \times 10^3$  kg. In Fig. 9B we plot the kinetic energy of the projectile as a function of the impactor diameter for different values of the impact speed. For the impactor diameters obtained above, we compute the corresponding kinetic energies, and, in Fig. 9B, we connect the points for the two different types of soils with dashed lines. For impact speeds in the range 3–6 km s<sup>-1</sup>, the range of kinetic energies at impact given by the dashed lines should be 0.8–2 tons TNT. For impact speeds below 1 km s<sup>-1</sup>, the kinetic energy is much lower than 1 ton TNT, either for dry or wet soil.

The previous estimates of the impact energy can be compared with other constraints coming from the energy of the airblast. Three types of blasts can be distinguished during the atmospheric entry of a meteoroid: the ballistic waves due to the supersonic mach cone created by the meteoroid's flight through the atmosphere, the explosion, and catastrophic fragmentation of the meteoroid in the atmosphere, and the explosion produced by the impact of the meteorite at the ground. Most of the kinetic energy is lost in the upper part of the atmosphere due to material ablation (heights over 20 km) and therefore only a small fraction of the initial energy is transferred into the fragmentation or crater formation blasts (Ceplecha et al. 1998).

The blasts recorded by the infrasound and seismic stations have already been independently analyzed by Brown et al. (2008) and Le Pichon et al. (2008). They both agree that the energy of the event producing the blasts was  $\sim 1\text{--}3$  tons TNT, though there is no conclusive evidence about which of the three possible sources mentioned above were registered. From the estimates of the backazimuth from the signal of the infrasound station of the International Monitoring System located in La Paz, Bolivia (I08BO), they both concluded that the blast was produced at or close to the impact site.

Energy coupled at the surface by the impact of the meteoroid on the ground was witnessed by several peasants of the community of Carancas as well as their animals. The impact produced an atmospheric shock followed by an expanding cloud of dust and debris, with the consequent local atmospheric overpressure. From interviews of several witnesses and information collected on the site, we have identified the following constraints to the overpressures as a function of distance from the crater:

- A man standing at  $\sim 400$  m from the crater site saw the expanding dust cloud, heard the explosion, but he did not suffer any injury; he also did not fall down (Fig. 10D).
- A man riding a bicycle at  $\sim 100$  m fell down and he felt a bit dizzy due to the explosion, but his eardrums were not ruptured. He was riding in a direction orthogonal to the line connecting to the crater (Fig. 10C).
- A bull similar to the Lidia bull-fighting breed at  $\sim 200$  m fell down and broke one of its horns. The bull weighed  $\sim 500$  kg (Fig. 10E).
- A mud shed with metal roof at  $\sim 120$  m from the crater was not seriously damaged. The shed has no glass windows. It received an impact from the ejecta that bent a metal sheet of the roof (Fig. 10B).

According to experiments with nuclear explosions (Glasstone and Dolan 1977), the minimum overpressure required to rupture the eardrum is 5 psi, and to produce moderate damage to wood houses is 2 psi. We estimate that the force required to cause a body to fall down is of the order of the force required to lift it, i.e., its weight. The force is given by the overpressure times the cross section of the body with respect to the shock wave. For a normal Aymara man (the native ethnic group in the Andes and Altiplano regions of southern Peru and Bolivia, height 1.6 m, weight 70 kg), the overpressure required to throw him down from his side is  $\sim 0.3$  psi, and from the front is  $\sim 0.15$  psi. For a  $\sim 500$  kg, 1.2 m height bull, the overpressure required at its side to turn it down is  $\sim 0.5$  psi. We acknowledge that these are rough estimates of the overpressures involved in the different cases, but taken together they are useful in providing an additional constraint on the magnitude of the explosion.

Based on data from U.S. nuclear explosion tests (Glasstone and Dolan 1977), Collins et al. (2005) obtain the following fitting function to the empirical data on the decay of peak atmospheric overpressure  $p$  (in Pa) with distance  $r_l$  (in m) for a 1 kiloton (kt TNT) surface burst:

$$p = \frac{p_x r_x}{4r_l} \left( 1 + 3 \left( \frac{r_x}{r_l} \right)^{1.3} \right). \quad (4)$$

where  $p_x$  is 75000 Pa and  $r_x = 290$  m (Collins et al. 2005). For an impact energy  $E$  (in kt TNT), the peak overpressure at a distance  $r$  is the same as that at a distance  $r_l$ , where  $r_l$  is given by  $r_l = r/E^{1/3}$ .

In Fig. 10, we put the location of the previous reports with respect to the crater as well as some constraints in the

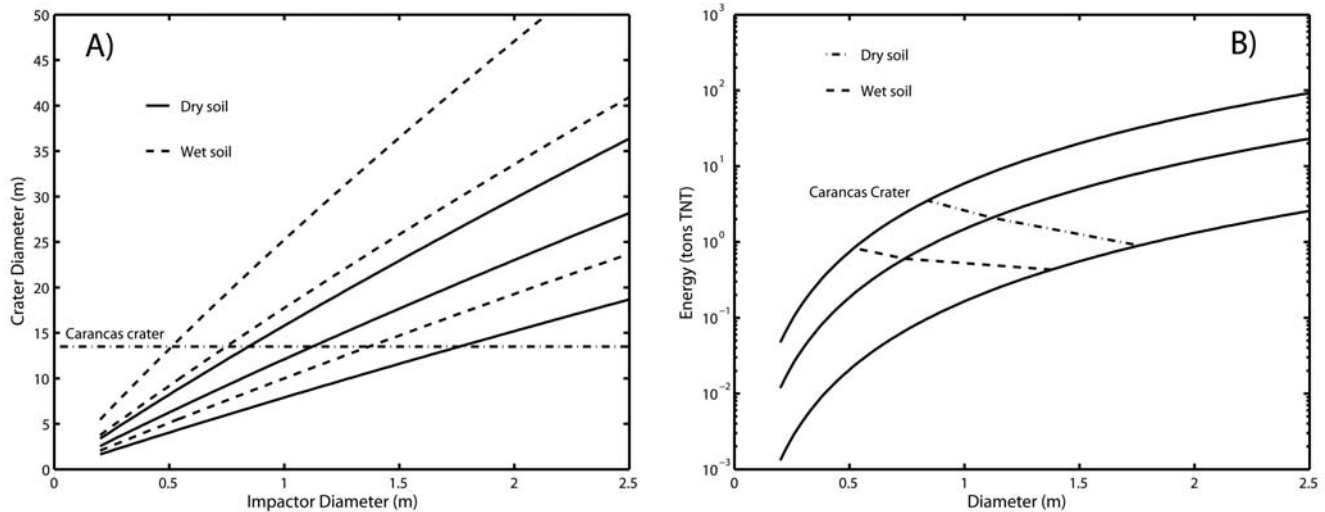


Fig. 9. Plot of the final crater diameter as a function of the impactor diameter calculated with the cratering laws of Holsapple and Housen (2007) for different impact speeds and target material. A horizontal line corresponding to a crater diameter of 13.5 m is also drawn. The solid lines correspond to an impact into a dry soil, while the dashed lines into a wet soil. For a given target material, the lines correspond from bottom to top to speeds of 1, 3 and 6 km s<sup>-1</sup>. B) Plot of the impact kinetic energy (in kton TNT) as a function of the impactor diameter for different impact speeds. The full lines correspond from bottom to top to impact speeds of 1, 3 and 6 km s<sup>-1</sup>, respectively. For the impactor diameters that create a crater diameter of 13.5, we compute the corresponding kinetic energies. Two lines for the two different target materials are drawn. The upper dash-dot line corresponds to an impact into a dry soil, while the lower dashed line into a wet soil.

overpressure experienced. We also plot circles at distances of 100, 200, 300 and 400 m from the crater and the corresponding peak overpressures for two different impact energies. The inner values correspond to 1 ton TNT and the outer values to 3 tons TNT, respectively. From the comparison of the reports and the expected peak overpressures, we conclude that impact energy in the range 1–3 tons TNT is consistent with the reports proximal to the crater.

In Fig. 10 we also plot the farthest ejecta found in different directions (stars) (Rosales et al. 2008). Since many pieces of ejecta were found between these points, the ejecta pattern can be represented by the envelope of these points. A shape close to SW-NE major axis ellipse can fit the points. The farthest ejecta in the NE direction were at ~130 m away, and in the SW direction they reached over ~350 m. The ejecta pattern is generally consistent with the E-W trajectory, though we can not ignore the effect of the pre-impact topography (the initial shock directed against the embankment) resulting in a ray of the grassy topsoil more orthogonal to the impact trajectory (Schultz et al. 2008). In order to reach the farthest distances, ejecta blocks of ~10 cm had to be ejected in ballistic trajectories from the crater at initial velocities up to ~40 m s<sup>-1</sup> in the NE direction and up to ~70 m s<sup>-1</sup> in the SW direction, including the effects of air drag. Ejecta directed downrange reflects the effect of the initial momentum at impact, as observed in many planetary settings. This led to an anisotropic distribution for Carancas (Fig. 10). Uprange ejecta, however, represents the explosive nature of the event (shock-induced excavation).

Explosion experiments compiled by Schoutens (1979)

indicate that an event needs to have an explosive energy greater than 2 tons TNT in order to have ballistic ejecta extending greater than 130 m. Taking into account the crater size and the characteristics of the impactor and the target, this energy range is only attainable with impact velocities over 3 km s<sup>-1</sup>.

One witness (Mr. R. Carbajal) observed the trajectory of the fireball from the roof of a house in Desaguadero. He was able to observe a single fireball from high in the sky until it disappeared at the horizon. During the entire flight the object had a luminous appearance, thereby indicating that aerodynamic ablation was maintained down to the surface. Light production in the lower atmosphere is known to stop only at velocities of ~3–4 km s<sup>-1</sup> (Ceplecha et al. 1998) supporting the evidence for a high impact speed and a single (or grouped) mass.

In order to estimate the possible outcome of a Carancas-like event at sea level, we model the evolution of the meteorite starting at 3800 m. We assume that at this height the ablation has almost stopped and the evolution can be considered as a dark flight (Ceplecha et al. 1998). The meteorite is subjected to the air drag and the acceleration of gravity. We model the evolution according to the equations of motion of a non-ablating body (equations 73–75 of Ceplecha et al. 1998). An important uncertainty originates from the unknown shape of the body and the associated drag coefficient. We assume speeds of 3 and 6 km s<sup>-1</sup> at 3800 m, terminal masses of 1 and 3 tons and drag coefficients of 1 (sphere) and 0.5 (streamline object). The evolution of the impact speed from 3800 m down to sea level is presented in Fig. 11. Note that a reduction of a factor of 1/2 in the drag

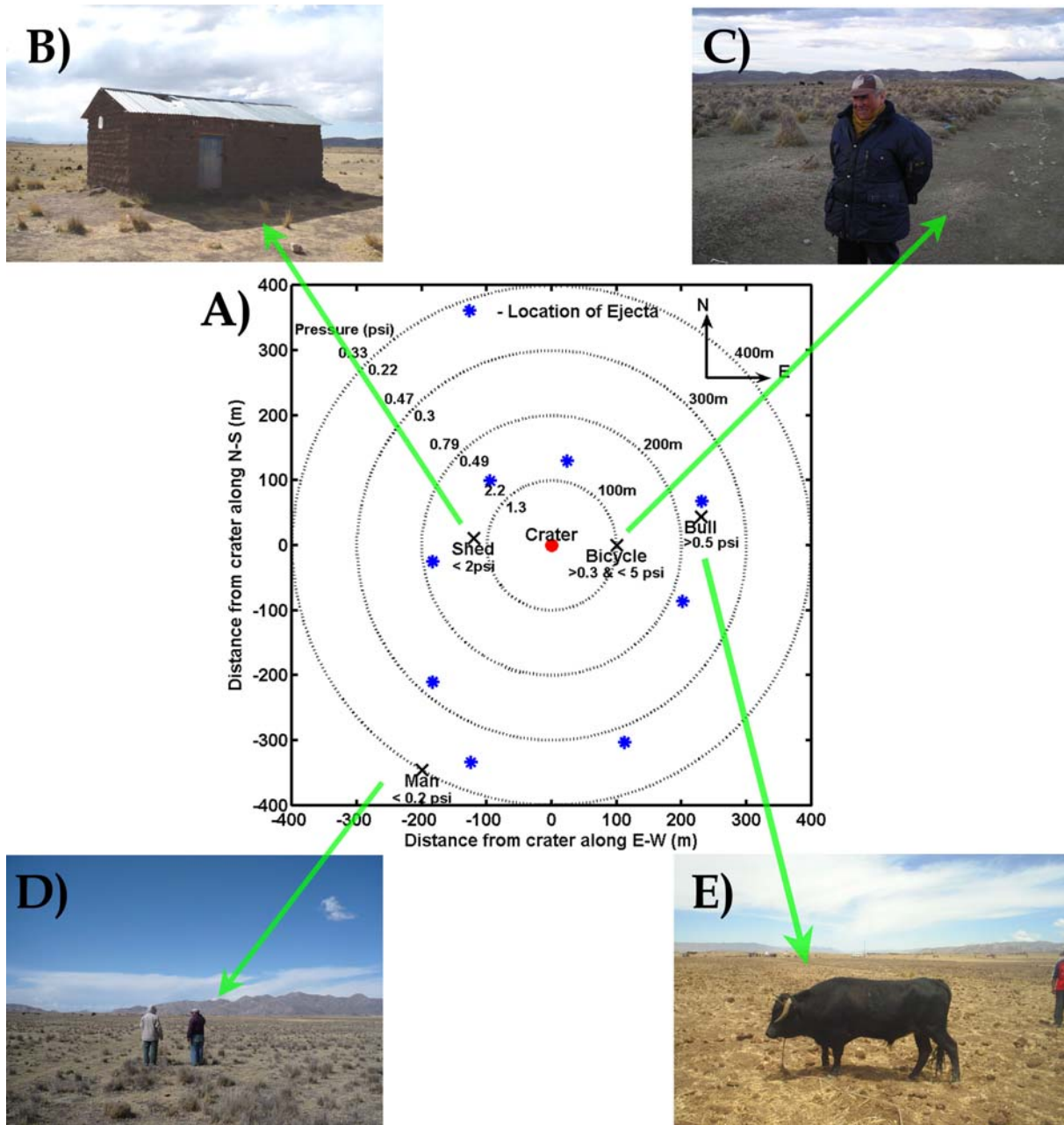


Fig. 10. A) Location of the reports listed in the text with the corresponding constraints in the overpressure experienced. We also plot circles at distance of 100, 200, 300, and 400 m from the crater and the corresponding peak overpressures for two different impact energies calculated with Equation 2. The blue stars correspond to the farthest ejecta that were found in different directions. B) A mud shed with metal roof which did not suffer any structural damage. It just received an impact from the ejecta that bent a metal sheet of the roof. C) Approximate location of the man that was riding a bicycle at the instant of impact. D) Mr. José Sarmiento (the man in the top right inset), who witnessed the impact and the expanding cloud of dust. This photo was taken a month after the impact, while he was interviewed by Mr. Pedro Miranda and G. T. He mentioned that the dust cloud covered the entire sky of this photo, up to an altitude higher than the cloud in the upper right. E) The bull, similar to the Lidia bull-fighting breed, with its left horn broken.

coefficient produces an increase by a factor  $\sim 2$  of the impact speed. We conclude that, though the meteorite suffers a large deceleration in the lower part of the atmosphere, it generally reaches the sea level with speeds over  $1 \text{ km s}^{-1}$ . According to Fig. 9A, the crater produced at sea level would still be around 8 to 10 m in diameter.

### The Seismic Energy and Efficiency

Le Pichon et al. (2008) derived a local seismic magnitude of  $ML = 1.45$  from the seismic recordings, corresponding to the maximum amplitude from the surface waves observed at BBOD. The seismic wave energy is obtained with the formula

of Gutenberg and Richter (1956):

$$\log E = 4.8 + 1.5M. \quad (5)$$

where the seismic energy ( $E$ ) is given in Joules. The seismic energy generated by the impact was  $\sim 9.4 \times 10^6$  J, equivalent to 2.3 kg TNT.

The seismic efficiency is defined as the ratio of the energy of the generated seismic waves to the kinetic energy of the meteorite. Since the impact energy was estimated to be in the range of 1 to 3 tons TNT, the seismic efficiency was on the order of  $10^{-3}$ . This is the first direct estimate of the seismic efficiency of an impact. Theoretical estimates of the seismic efficiency were done by Shishkin (2007). He obtained values on the order of  $10^{-2}$  in the case of low-speed and small impacts, in general correspondence with our empirical estimate. According to his results, the seismic efficiency is expected to decrease substantially with increasing impact speed and size of the impactor.

Media reports mentioned that several persons experienced a small earth tremor and there were reports that windows were broken (see Media Reports in the Reference List). In one of our visits, G. T. and J. I. canvassed the area asking if any window was broken due to the event. Let us note that most of the constructions in the impact area are mud sheds like the one shown in Fig. 10B. Those sheds do not have windows or they are very small. However, a few houses at distances of a few hundred meters from the crater have experienced breakage of window glass. In particular, the School of Huanocollo suffered cracked and broken windows on one of its buildings due to the impact. The windows in the buildings with thick mud walls were intact, while the windows in the building with thin brick walls had suffered considerable damage, despite the fact that both sets of windows would have been exposed to similar blast overpressures. The thin windows had very thin glass only 1mm thick. The School of Huanocollo is 1300 m from the crater.

The atmospheric overpressure required for glass breakage has been estimated to be at least on the order of 0.5 to 1 psi (Glasstone and Dolan 1977), either for large or small windows. For a 1 to 3 ton TNT explosion, the peak overpressure at the distance of the School should have been below 0.1 psi (Equation 4), not enough to produce glass breakage. Nevertheless, the earth tremor produced by the seismic wave may have been enough to crack the glass in a weak structure. The maximum amplitude of the surface wave was  $\sim 1$  mm at station BBOD at 47 km from the impact point (see Fig. 3B). The Prague formula (Vanek et al. 1962) predicts an attenuation of the amplitude of the seismic wave that goes with  $r^{-1.66}$ ; while an equation derived from the analysis of surface explosions in the United States (Navarro and Brockman 1970) and useful at short distance range (less than 200 km) predicts an attenuation proportional to  $r^{-2.3}$ . Using these two relations, we can estimate that the maximum

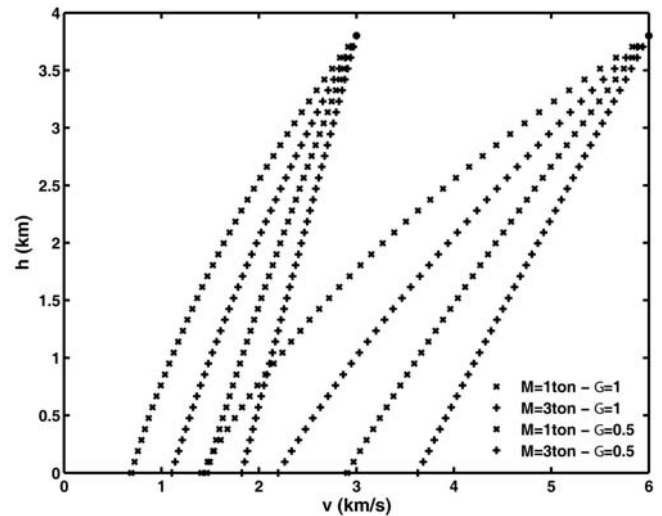


Fig. 11. The speed of a falling body as a function of the altitude over the ground. The body initially had a velocity of 3 and 6  $\text{km s}^{-1}$  at 3800 m over sea level and an entry angle of  $50^\circ$ . We assume no ablation and the evolution can be considered as a dark flight according to the equations presented in Ceplecha et al. (1998). Two set of masses are considered (1 and 3 tons) as well as two different drag coefficients ( $G = 1$  and  $0.5$  corresponding a sphere and streamline object, respectively). The left group of lines corresponds to the initial velocity of  $3 \text{ km s}^{-1}$ , while the right group has initial velocities of  $6 \text{ km/s}$ .

amplitude of the seismic wave expected at the location of the School ranges from 0.4 to 4 mm. These amplitudes might be enough to crack a very brittle 1 mm thick glass, particularly if the associated ground velocities (and accelerations) were high as would be expected near the crater.

### Other Recent Terrestrial Craters

Only a few of the close to  $\sim$ thousand recorded meteorite falls have produced noticeable marks when they reach the ground. In Table 1 we review the information about the most relevant impact structures in recent history. The two largest holes produced by chondrite falls (Kunya-Urgench and Jilin) are clearly penetration pits with a depth to diameter ratio over 1 (Mukhamednazarov 1999; Academia Sinica 1977). The iron fall of Sterlitamak was tentatively classified as a transitional morphological type between a meteorite crater and an impact pit (Petaev 1992). Only two cases might indicate shock-generated craters: individual craters within the Sikhote-Alin (Krinov 1971) or Campo del Cielo (Cassidy et al. 1965; Wright et al. 2006, 2007) strewn fields, both produced by strong iron meteorites. Such craters are often called “explosion” craters due to their sudden transfer of energy and momentum into the target. The largest crater formed in the multiple iron fall of Sikhote-Alin (Krinov 1971) was 26.5 m in diameter and 6 m deep, with the typical value of the depth to diameter ratio of  $\sim 0.2$  for impact craters and containing relict iron masses. Nevertheless, there is no information

concerning the presence of shock metamorphic features in the target minerals. Hence, it is not possible to assess the peak pressure, temperature, or impact speed. There also was neither seismic or infrasonic record of that event. Although the fireball was observed in a huge area, there was no witness of crater formation. Recent studies of the Campo del Cielo crater field also indicate several craters formed “explosively” (Wright et al. 2006, 2007), although shocked materials have not yet been identified. Consequently, possible impact craters have been formed in historical times, but were produced by strong iron masses rather than weak chondritic objects as at Carancas.

### REPORTED HEALTH PROBLEMS

The Carancas event received much attention from the media because, in early reports, it was mentioned that hundreds of people became sick after being close to the crater (see Media Reports in References). Since it was the first time that the formation of a crater was witnessed by many people and there were many visitors just a few minutes after the impact, we decided to look into the possible health risks posed by a small impact through investigation of these alleged health problems.

The media reports mentioned that hundreds of people visited the Local Health Center of Carancas affected by headache, vomiting, and stomachaches. In particular, a few policemen that were inside the crater were attended in the Hospital of Desaguadero and in the Sanity Police Hospital in Puno, Peru. Only oxygen and hydration was provided to them. G. T and J. I. interviewed the nurse in charge of the Health Center in October 2008, Mrs. Nérida Chanía. She said that in the first days after the impact nobody from the community approached the Center mentioning any symptoms as a consequence of visiting the crater. It was only after it was announced publicly that a group of Physicians and Nurses from the Regional Capital of Puno would visit the Community of Carancas to give treatment to the people affected by the crater, that approximately 180 people approached the Health Center mentioning that they were suffering the symptoms listed above. The nurse described a rumor which circulated among the villagers to the effect that anyone reporting some kind of sickness related to the crater formation would get free health care. Thus it seems most plausible to us that local residents were mainly interested in getting free medicine and health support in a remote rural area where both are hard to come by.

Blood and urine tests were done for 11 persons of the community of Carancas by the Dirección Regional de Salud de Puno (DIRESA). J. B. interviewed them afterwards and it turned out that some of them were never close to the crater in the first days after the impact. In all studied cases, the concentrations of lead in blood were acceptable for persons not exposed to lead at work. Large contents of arsenic (over 200 mg As per liter of urine) were found in a few cases. These

values are over the limit for biological tolerance for human exposed to arsenic at work. DIRESA also took samples of water from inside the crater and from several water wells from where the studied persons take the drinking water. A large content of arsenic was found in a few samples, in correspondence with the location of the people with arsenic poisoning. The arsenic content of the water inside the crater was lower than in the wells.

We conclude that there is no firm evidence to suggest that more than a few (if any) persons were affected by the underground trapped gases that were released at impact, the gases having bubbled through the water deposited in the crater floor. Most of the alleged health problems were a consequence of mass hysteria and people seeking free medical support for pre-existing conditions.

### COMPARISON WITH OTHER CASES AND MODELS

Some models for atmospheric entry of large meteoroids describe the disruption followed by lateral dispersal and deformation of the interacting atmospheric Mach cone, thereby producing a pancake-like assemblage of fragments (Bland and Artemieva 2003; Chyba et al. 1993). Larger objects are able to produce crater fields such as Campo del Cielo (Cassidy et al. 1965) or Sikhote-Alin (Krinov 1971), whereas smaller objects produce meteorite strewn fields after decelerating to low terminal velocity such as those described by Jilin (Academia Sinica 1977). The material strength of the meteoroid plays an important role in the fate of the object during atmospheric flight. Based on standard ablation theory, it is widely accepted that only iron meteorites (initially a few meters in diameter) are strong enough to survive atmospheric entry and produce small craters. Stony masses need to exceed  $\sim 10^{10}$  kg in order to survive entry with speeds  $>14$  km  $s^{-1}$ , whereas a mass less than  $10^8$  kg will undergo catastrophic disruption at high altitude (Bland and Artemieva 2003, 2006). Smaller masses produce a swarm of meteorites that impact the Earth's surface at low terminal velocities (100–300 m  $s^{-1}$ ). The limiting survival masses for iron objects are much lower. For example, iron meteoroids of  $10^5$  kg could retain a large fraction of their original mass as well as a large fraction of the original velocity. But iron meteoroids only represent 3% of the objects that strike the upper atmosphere (Ceplecha et al. 1998).

Of the known contemporary meteorite craters (Table 1), only the largest craters in the Sikhote-Alin and Campo del Cielo strewn fields (iron meteoroids) can be considered true impact craters. The Carancas meteorite crater is therefore a puzzling case: a stony mass of several tons entering the upper atmosphere with a speed between 12–16 km  $s^{-1}$  and surviving intact or undispersed. In spite of significant ablation, it did not catastrophically disrupt and disperse during its atmospheric entry. A large fraction of the original mass ( $\sim 1$  ton) impacted the ground at an altitude of  $\sim 3800$  m. The impact speed was over 3 km  $s^{-1}$  and the kinetic energy ranged from 1 to 3 tons

TNT. The meteorite penetrated deeply into the subsurface and it was largely destroyed. The explosive impact crater ejected a volume of sediment many times larger than the original meteorite.

The meteoroid entry for the Carancas has been simulated (Brown et al. 2008; Borovička and Spurný 2008) by using the model developed by Revelle (2005) and Cepelcha et al. (1998). These models include ablation but for the cited works which modelled the Carancas object, fragmentation was explicitly ignored. According to these results a monolithic meteoroid may have avoided fragmentation if the tensile strength had been higher than most observed meteoroids (20–40 MPa, Borovička and Spurný 2008). Unfortunately, there is no measure of the strength of the meteoritic material from the recovered samples so far. Furthermore, that material has been subject to shock and disaggregation and hence does not represent the material properties of the pre-atmospheric meteoroid. That a spread in strengths of pre-atmospheric meteoroids is expected is hardly surprising; the stress fracture data of meteorites in the lab show a more than one order of magnitude spread, underlining the individuality of each object (cf. Petrovic 2001). Another factor that might affect the ablation process is the shape of the meteoroid. This concept of a range of strength values should be applied by modelers to ablation studies of meteoroids to explore the end member states of the ablation process given the large spread in observed fireball strengths and meteorite strengths (rather than a fixed average), as well as several possible shapes of the meteoroids. The size dependency of these parameters is another factor to take into account; although it is plausible that meter-size monolithic meteoroid with high strength might exist, as meteorite size increases, the probability of large flaws existing increases and the global strength is greatly reduced.

The high altitude of the area might have played role in the outcome of this event, but not a crucial one. Even if the Carancas meteorite had continued to sea level, it still would have produced a significant crater (Fig. 11).

Kenkmann et al. (2008) applied the model of Bland and Artemieva (2003) to the case of Carancas. They modeled the atmospheric entry and subsequent disruption of a meteoroid by varying the mass and internal strength. They favor a solution with an initial 1.9 tons meteoroid and high strength; after the atmospheric passage, the largest fragment (0.7 m–700 kg) impacts the surface at  $180 \text{ m s}^{-1}$  (for an altitude of 3800 m), and it produces a single  $\sim 10 \text{ m}$  crater. The corresponding impact energy is 0.02 tons TNT. These predictions are generally consistent with expectations prior to this collision but are in contradiction with results presented in this paper as well as initial petrologic evidence (Harris et al. 2008a). In particular, we have presented several estimates of the impact energy in the range 1–3 tons TNT based on different and independent data, a value two orders of magnitude larger than their results. Moreover, their model is

predicated on a very low entry angle (less than 15 degrees from the horizontal) for the Carancas meteoroid to avoid fragmentation; this is strong contradiction to the results independently derived by Le Pichon et al. (2009) and Brown et al. (2008) which suggest steep angles from examination of the observational data.

While the standard pancake model (Chyba et al. 1993) or the separate fragment model (Bland and Artemieva 2003, 2006) may apply to relatively strong meteoritic bodies (irons), such descriptions may need to be modified for weaker objects like stony meteorites, in order to explain the Carancas case (Schultz et al. 2008). For example, experimental studies have demonstrated that catastrophically disrupted hypervelocity projectiles will laterally disperse while passing through a thin atmosphere; however, at high atmospheric pressures, the trailing shock confines smaller fragmented masses within the Mach cone (Schultz 1992; Schultz et al. 2008). According to this model, the Carancas meteorite “gently” disrupted but did not laterally disperse. There is still much work to do to understand this event in terms of the existing models.

The Carancas impact raises the possibility that there may be many more unrecognized small craters produced by stony meteorites. Two-meter diameter stony meteorites enter the upper atmosphere at a rate of  $\sim 8$  objects per year (Bland and Artemieva 2003). As an extreme example, if the flight behavior and impact effects demonstrated by the Carancas impact apply to all other stony meteoroids of similar size, (a situation we do not expect to be typical according to the previous considerations), then the current impact rate places a very upper limit for similar encounters at one event every thousand years in an area of  $\sim 70,000 \text{ km}^2$ . While large buried iron masses are easy to detect, the Carancas impact illustrates how stony meteorites fully fragment and pulverize at impact and become intimately mixed with the ground. Surviving fines are then highly susceptible to chemical weathering and can easily get lost in sediments below the floor of a nondescript depression.

## CONCLUSIONS

From our re-analysis and interpretation based in part on the earlier works of Le Pichon et al. (2009) and Brown et al. (2008), we conclude that the key results regarding this unusual crater-forming impact event are as follows:

- The initial mass of the meteoroid before entering the atmosphere was from 7 to 12 metric tons, the corresponding initial diameter was from 1.6 to 2 m.
- The initial velocity was in the range 12 to  $17 \text{ km s}^{-1}$ , and the initial kinetic energy was in the range 0.12 to 0.41 kT TNT.
- The trajectory had an azimuth in the range  $80^\circ$  to  $110^\circ$ , and an inclination measured from the horizontal between  $45^\circ$  and  $60^\circ$ .



- The heliocentric orbit of the meteoroid was compatible with the orbits of known near-Earth asteroids.
- The passage of the fireball through the atmosphere and the explosion at impact was detected by seismic and infrasound detectors.
- The impact produced the first unambiguous seismic recording of such event on Earth.
- The impact time deduced from the arrival times of the crustal P-seismic waves was 16:40:14.4 UT.
- The seismic efficiency was on the order of  $10^{-3}$ .
- Window glasses were broken due to the seismic wave.
- A crater of 13.5 m (rim-to-rim) was formed, with a depth to diameter ratio of  $\sim 0.2$ , typical of impact craters.
- Several samples of stony meteorites were collected inside and outside the crater. The meteorites were classified as H4–5 ordinary chondrite.
- The petrological analysis of minerals presented in the ejecta deposits indicate levels of shock metamorphism compatible with peak pressures at impact over several GPa.
- The impact energy was independently estimated using different sets of data, including: the blasts recorded by the infrasound and seismic stations, the effects of the atmospheric shock wave on several witnesses, and the distribution of the ejecta. All these estimates agree on a value for the impact energy in the range  $\sim 1$ –3 tons TNT.
- The impact velocity on the ground was higher than  $\sim 3 \text{ km s}^{-1}$ , but lower than  $6 \text{ km s}^{-1}$ .
- The crater was formed as a consequence of a hypervelocity impact event (impact speed larger than the speed of sound in the material target).
- In spite of significant ablation, the meteoroid did not catastrophically disrupt and/or disperse during its atmospheric entry.
- The mass of the impactor was in the range 0.3 to 3 ton, and the diameter was 0.6 to 1.1 m.
- There are no definitive indications of large remnants of the meteorite inside the crater.
- The health problems reported in the media were greatly exaggerated.

*Acknowledgments*—We appreciate the hospitality of the Universidad Nacional del Altiplano and the Gobierno Regional de Puno, Peru. We thank them for being an inviting host and providing us with logistical support. We thank the villagers of Carancas for taking care of the crater and we support their efforts to preserve the site. Some samples and witnesses testimonies were provided by Pedro Miranda and Gonzalo Pereira, from Planetario Max Schreier, La Paz, Bolivia. Many other colleagues from different Peruvian institutes like Instituto Geofísico del Perú (IGP), Instituto Geológico Minero y Metalúrgico (INGEMMET) and Comisión Nacional de Investigación y Desarrollo Aeroespacial (CONIDA) have collaborated with our work

and they have provided useful information. We also thank Dr. Franz Brandstätter from Naturhistorisches Museum (Vienna, Austria) to provide access to the equipment for the analysis of the meteorite. G. Tancredi thanks the discussions with Ernesto Blanco (Grupo Biomecanica, Fac. Ciencias, Uruguay) and Sofia Favre on the biomechanics of lifting bodies and the analysis of the overpressure constraints. He also thanks R. Bowley (Fac. Veterinaria, Uruguay) for the information about the characteristics of the bull. Fieldwork was supported in part by the Mary Hill and Bevan M. French Fund for Impact Geology. The insightful comments by reviewers Clark Chapman, Gareth Collins, and Gordon Osinski helped to improve an earlier version of this work and are greatly appreciated.

Color versions of the photographs can be obtained at: <http://www.astronomia.edu.uy/Carancas>.

*Editorial Handling*—Dr. Nancy Chabot

## REFERENCES

- Bland P. and Artemieva N. 2003. Efficient disruption of small asteroids by Earth's atmosphere. *Nature* 424:288–291.
- Bland P. and Artemieva N. 2006. The rate of small impacts on Earth. *Meteoritics & Planetary Science* 41:607–663.
- Borovička J. and Spurný P. 2008. The Carancas meteorite impact—Encounter with a monolithic meteoroid. *Astronomy & Astrophysics* 485:L1–L4.
- Bowell E. and Muinonen K. 1994. Earth-crossing asteroids and Comets: Ground-based search strategies. In *Hazards due to comets and asteroids*, edited by Gehrels T., Matthews M. S., and Schumann A. Tucson: The University of Arizona Press. 149 p.
- Breiner S. 1999. *Applications manual for portable magnetometers*. San Jose, California: Geometrics. 58 p.
- Britt D. and Consolmagno G. 2003. Stony meteorite porosities and densities: A review of the data through 2001. *Meteoritics & Planetary Science* 38:1161–1180.
- Brown P., Sukara E. A., ReVelle D. O., Edwards W. N., Arrowsmith S., Jackson L., Tancredi G., and Eaton D. 2008. Analysis of a crater-forming meteorite impact in Peru. *Journal Geophysical Research—Planets* 113:E09007.
- Cassidy W., Villar L. M., Bunch T., Kohman T., and Milton D. 1965. Meteorites and craters of Campo del Cielo, Argentina. *Science* 149:1055–1064.
- Cepelcha Z., Borovička J., Elford W., ReVelle D., Hawkes R., Porubčan V., and Šimek M. 1998. Meteor phenomena and bodies. *Space Science Reviews* 84:327–471.
- Chyba C., Thomas P., and Zahnle K. 1993. The 1908 Tunguska explosion—Atmospheric disruption of a stony asteroid. *Nature* 361:40–44.
- Collins G., Melosh H., and Marcus R. 2005. Earth Impact Effects Program: A Web-based computer program for calculating the regional environmental consequences of a meteoroid impact on Earth. *Meteoritics & Planetary Science* 40:817–840.
- Connolly H. 2007. Meteoritical Bulletin, No. 93, 2008 March. *Meteoritics & Planetary Science* 43:571–632.
- Glasstone S. and Dolan P. 1977. *The effects of nuclear weapons*, 3rd ed. Washington D.C.: United States Department of Defense and Department of Energy. 653 p.

- Hedlin M., Degroot-Hedlin C., Walker K., Drob D., and Zumbege M. 2008. Study of infrasound propagation from the shuttle Atlantis using a large seismic network. *Journal of the Acoustic Society of America* 123:3829.
- Harris R. S.; Schultz P. H.; Tancredi G.; and Ishitsuka J. 2008a. Preliminary petrologic analysis of impact deformation in the Carancas (Peru) cratering event. 39th Lunar and Planetary Science Conference. Abstract #2446.
- Harris R. S.; Schultz P. H.; Tancredi G., and Ishitsuka J. 2008b. Petrology of ejecta from the Carancas (Peru) crater: Insights into the dynamics of an “unusual” impact event. *Asteroids, Comets, Meteors 2008*. LPI Contribution No. 1405, p. 8302.
- Holsapple K. 2003. Theory and equations for crater scaling. <http://keith.a.washington.edu/craterdata/scaling/index.htm>.
- Holsapple K. and Housen K. 2007. A crater and its ejecta: An interpretation of Deep Impact. *Icarus* 187:345–356.
- Joint investigation group of the Kirin Meteorite Shower Academia Sinica. 1977. A preliminary survey on the Kirin Meteorite Shower. *Scientia Sinica* 4:502–512.
- Kanamori H., Mori J., Anderson D. L., and Heaton T. H. 1991. Seismic excitation by the space shuttle Columbia. *Nature* 349:781–782.
- Kenkmann T., Artemieva N., and Poelchau M. 2008. The Carancas event on September 15, 2007: meteorite fall, impact conditions, and crater characteristics. 39th Lunar and Planetary Science Conference. Abstract #1094.
- Krinov E. 1971. New studies of the Sikhote-Alin iron meteorite shower. *Meteoritics* 6:127–138.
- Lillie R. 1999. *Whole Earth geophysics*. New York: Prentice Hall. 63 p.
- Le Pichon A., Antier K., Cansi Y., Hernandez B., Minaya E., Burgoa B., Drob D., Evers L.G., and Vaubaillon J. 2008. Evidence of a meteoritic origin of the September 15, 2007, Carancas crater. *Meteoritics & Planetary Science* 43:1797–1809.
- Macedo L. F. and Macharé J. O. 2007. The Carancas meteorite fall, 15 September 2007. Official INGEMMET initial report. Released 21 September 2007.
- Media Reports: Diario La Republica Online—An extended coverage in many online articles at <http://www.larepublica.com.pe>. For example, “600 afectados en Puno por caída de meteorite” (09/19/2007), [http://www.larepublica.com.pe/component?option=com\\_contentant/task/view/id,178836/Itemid,0/Boletin de Noticias del Gobierno Municipal de Puno \(09/18/2007\)](http://www.larepublica.com.pe/component?option=com_contentant/task/view/id,178836/Itemid,0/Boletin%20de%20Noticias%20del%20Gobierno%20Municipal%20de%20Puno%20(09/18/2007)), <http://www.munipuno.gob.pe/noticiasview.php?op=leer&id=533>.
- Chandler D. 2008. Meteorites: How big is safe? *New Scientist* 2641:40–43. *Nature*, vol. 449, p. 390. 2007. Meteorite proves to be a hit in Peru.
- Minaya E., Rougon P., Valero D., Fernández G., Lazaro E., and Cano W. 2007. *Eos Transactions* 8. Abstract S34A-02.
- Mukhamednazarov S. 1999. Observation of a fireball and the fall of the first large meteorite in Turkmenistan. *Astronomy Letters* 25:117–118.
- Navarro R. and Brockman F. 1970. Seismic activity in September 1969 near Ruliston test site. USGS Publication No. 746–5.
- Petaev M. 1992. The Sterlitamak meteorite, a new crater-forming fall. *Astronomicheskii Vestnik* 26:82–99.
- Petrovic J. 2001. Review: Mechanical properties of meteorites and their constituents. *Journal of Materials Science* 36:1579–1583.
- ReVelle D. 2005. Recent advances in bolide entry modeling: A bolide potpourri. earth, moon, and *Planets* 97:1–35.
- Rosales D., Vidal E., Ishitsuka J., and Benavente S. 2008. Geomagnetic study of the Carancas meteorite and its crater. 39th Lunar and Planetary Science Conference. Abstract #1744.
- Schoutens J. 1979. *Nuclear geoplosics sourcebook*, vol. IV, part II. Defense Nuclear Agency. p. IV-4–IV-127.
- Schultz P. H. 1992. Atmospheric effects on ejecta emplacement and crater formation on Venus from Magellan. *Journal of Geophysical Research* 97(E10):16,183–16,248.
- Schultz P. H., Harris R. S., Tancredi G., and Ishitsuka J. 2008. Implications of the Carancas meteorite impact. 39th Lunar and Planetary Science Conference. Abstract #2409.
- Shishkin N. 2007. Seismic efficiency of a contact explosion and a high-velocity impact. *Journal of Applied Mechanics and Technical Physics* 48:145–152.
- Stöffler D. and Langenhorst F. 1994. Shock metamorphism of quartz in nature and experiment: I. Basic observation and theory. *Meteoritics* 29:155–181.
- Stöffler D., Gault D., Wedekind J., and Polkowski G. 1975. Experimental hypervelocity impact into quartz sand—Distribution and shock metamorphism of ejecta. *Journal Geophysical Research* 80:4062–4077.
- Tancredi G. 2006. From where in the sky do they come? Abstract. *IAU Symposium 236 “Near-Earth Objects.”*
- Tancredi G., Ishitsuka J., Rosales D., Vidal E., Dalmau A., Pavel D., Benavente S., Miranda P., Pereira G., Vallejos V., Varela M. E., Brandstätter F., Schultz P. H., Harris R. S., and Sánchez L. 2008. What do we know about the “Carancas-Desaguadero” fireball, meteorite and impact crater? 39th Lunar and Planetary Science Conference. Abstract #1216.
- Vanek J., Zátpek A., Kárník V., Kondorskaya N., Riznichenko Y., Savarensky E., Solov’ev S., and Shebalin N. 1962. Standardization of magnitude scale. *Izvestia Akademii Nauk, Seriya Geofizitsekaya* 2, pp. 153–158.
- Wetherill G. and Revelle D. 1981. Which fireballs are meteorites—A study of the Prairie Network photographic meteor data. *Icarus* 48:308–328.
- Wright S., Vesconi M., Gustin A., Williams K., Ocampo A., and Cassidy W. 2006. Revisiting the Campo Del Cielo, Argentina crater field: A new data point from a Natural Laboratory of Multiple Low Velocity, Oblique Impacts (abstract). 37th Lunar and Planetary Science Conference.
- Wright S., Vesconi M., Spagnuolo M., Cerutti C., Jacob R., and Cassidy W. 2007. Explosion craters and penetration funnels in the Campo Del Cielo, Argentina crater field. 38th Lunar and Planetary Science Conference. Abstract #2017.
- Yuan X., Sobolev S., Kind R. 2002. Moho topography in the central Andes and its geodynamic implications. *Earth and Planetary Science Letters* 199:389–402.